Nuclear Engineering and Technology xxx (xxxx) xxx

Contents lists available at ScienceDirect

Nuclear Engineering and Technology

journal homepage: www.elsevier.com/locate/net

Original Article

Hydrothermal synthesis, structure and sorption performance to cesium and strontium ions of nanostructured magnetic zeolite composites

Artur Dran'kov [a, **], Oleg Shichalin [a, *], Evgeniy Papynov [a], Alexey Nomerovskii [a], Vitaliy Mayorov [a], Vladimir Pechnikov [a], Andrei Ivanets [b], Igor Buravlev [a], Sofiya Yarusova [c], Alexey Zavjalov [d], Aleksey Ognev [a], Valeriya Balybina [a], Aleksey Lembikov [a], Ivan Tananaev [a, e], Nikolay Shapkin [a]

[a] Far Eastern Federal University, 10 Ajax Bay, Russky Island, 690922, Vladivostok, Russia
[b] Institute of General and Inorganic Chemistry of National Academy of Sciences of Belarus, Surganova st. 9/1, Minsk, 220072, Belarus
[c] Vladivostok State University of Economics and Service, Gogolya st., 41 Vladivostok, 690014, Russia
[d] Institute of Solid State Chemistry and Mechanochemistry of the Siberian Branch of the Russian Academy of Sciences, 18, st. Kutateladze, Novosibirsk, 630128, Russia
[e] Ozersk Technological Institute, Branch of NRNU MEPhI, Ozersk, 456780, Russia

ARTICLE INFO

Article history:
Received 27 September 2021
Received in revised form
6 December 2021
Accepted 7 December 2021
Available online xxx

Keywords:
Zeolite adsorbents
Magnetic composites
Hydrothermal synthesis
Cesium and strontium radionuclides
Water treatment

ABSTRACT

The problem of water contamination by long-living cesium and strontium radionuclides is an urgent environmental issue. The development of facile and efficient technologies based on nanostructured adsorbents is a perspective for selective radionuclides removal. In this regard, current work aimed to obtain the nanostructured magnetic zeolite composites with high adsorption performance to cesium and strontium ions. The optimal conditions of hydrothermal synthesis were established based on XRD, SEM-EDX, N_2 adsorption-desorption, VSM, and batch adsorption experiment data. The role of chemical composition, textural characteristics, and surface morphology was demonstrated. The monolayer ion-exchange mechanism was proposed based on adsorption isotherm modeling. The highest Langmuir adsorption capacity of 229.6 and 105.1 mg/g towards cesium and strontium ions was reached for composite obtained at 90 °C hydrothermal treatment. It was shown that magnetic characteristics of zeolite composites allowing to separate spent adsorbents by a magnet from aqueous solutions.

1. Introduction

The inorganic synthesis of functional materials for radiochemistry tasks makes an important contribution to improving the efficiency and safety of radioactive waste management technologies, which is associated with the need for the development and production of highly effective sorbents for the ^{137}Cs and ^{90}Sr radionuclides removal from gas and liquid media [1–4]. These are the most hazardous isotopes with a long half-life, which represent the basis of irradiated nuclear fuel and make the main contribution in terms of a specific activity to the composition of RW [5,6]. The risk of their possible release into the environment poses a special threat of radiation contamination of large areas due to their high migration ability in air, water, and soil [7].

Technologies for LRW treatment from ^{137}Cs and ^{90}Sr with a high degree of efficiency are implemented based on sorption processes, including the use of ion-exchange synthetic zeolites [8–10]. These are inorganic materials of aluminosilicate composition with a specific frame structure consisting of tetrahedral silicon dioxide and aluminum oxide separated by oxygen atoms, including ion-exchange cations Na^+, K^+, Ca^{2+}, and Mg^{2+} [11–13]. Zeolites have a highly porous structure [14], radiation [15] and thermal [16] stability, high ion-exchange capacity, and selectivity to several radionuclides, as described in detail in a broad review by Jiménez-Reyes et al. [17]. The sorption efficiency of synthetic zeolites for the

* Corresponding author.
** Corresponding author.
E-mail addresses: artur.drankov@gmail.com (A. Dran'kov), oleg_shich@mail.ru (O. Shichalin).

https://doi.org/10.1016/j.net.2021.12.010

^{137}Cs and ^{90}Sr removal was also evaluated in many studies [18–21], which proved the prospects of such sorbents. For example, such sorbents have found practical application in the course of eliminating the consequences of the accident at the Fukushima-1 nuclear power plant in 2011 in Japan at the stage of preliminary purification of contaminated seawater used for additional cooling of emergency power units of the plant [22,23]. In addition, zeolites are excellent candidates for the formation of dense ceramic and glass-ceramic matrices for curing spent forms of sorbents for reliable and safe radionuclides immobilization [24–29] and radioisotope products producing [30].

Recently, considerable attention has been paid to the synthesis of nanostructured crystalline zeolites to increase the specific surface area, change the configuration of the porous structure, as well as change the chemical composition [31]. In this case, it was possible to impregnate the required ion-exchange cations with an increase in their concentration in the sorbent composition, an increase in their penetrating ability, and diffusion rate during the exchange with other cations from solutions.

Despite these advantages of highly dispersed zeolites, there is a serious problem of their separation from the solution being cleaned. The traditional method of high-performance centrifugation is long and expensive to implement, and also does not always lead to the desired result and in some cases leads to the use of additional separation methods, which may even lead to the formation of secondary waste. As an alternative, it was proposed to use the magnetic separation method, which is more efficient, simple, and fast to implement [32]. However, this method applies only to those sorbents that can be magnetized in an external magnetic field and have a sufficient magnetic moment to be controlled when it is applied.

Similar examples of sorbents with magnetic properties are composite materials based on zeolites in composition with magnetic phases, for example, with iron oxides or metallic iron. In particular, Bourlinos et al. The outer surface of Y zeolite was modified under hydrothermal conditions with maghemite, and the resulting material was used for Hg^{2+} adsorption [33]. Oliveira et al. [34] proposed a method for direct deposition of maghemite on the surface of NaY zeolite for the sorption of Cr^{3+}, Cu^{2+}, and Zn^{2+} ions from aqueous media. Faghihian et al. [35] synthesized a magnetic composite by chemical co-deposition of Fe^{2+} and Fe^{3+} in the presence of A zeolite and evaluated the adsorption efficiency to Cs^{+} and Sr^{2+}. The method of impregnation of metallic iron nanoparticles into a zeolite volume was described in Falyouna et al. [36] and was successfully applied to the sorption of Cs^{+} ions. Nanostructured magnetic zeolites have also been synthesized and studied in such works as Eljamal et al. [37], Shubair et al. [38], and Rahman et al. [39] by similar methods of reducing precipitation of magnetic iron nanoparticles in the presence of commercial zeolite. Faghihian et al. [40] by wet synthesis by mixing solutions of precursors forming zeolite A in composition with magnetite nanoparticles; O. A. Abdel Moamen et al. [41] by impregnating magnetite nanoparticles into the volume of nanoscale particles of Y zeolite, previously obtained under hydrothermal conditions. In these works, it was shown that the selective Cs^{+} and Sr^{2+} removal, as simulators of unstable isotopes of these elements, proceeded efficiently, taking into account the composition of the purified medium, as well as preserving the magnetic characteristics of materials controlled by an external magnetic field, which proves the high practical prospects of such sorbents. Lihareva N. [42] evaluated the removal of Cs^{+} and Sr^{2+} from aqueous solutions using a clinoptilolite. The kinetic data were fitted to the pseudo-second-order. The isotherm data were best adjusted to the Langmuir model with a maximum adsorption capacity of 122.7 and 21.50 mg/g for Cs^{+} and Sr^{2+}, respectively showing an ion-exchange mechanism. Due to the cations' ionic radii and the water content and frameworks, cesium prefers to be adsorbed onto natural zeolites, mainly chabazite and clinoptilolite; on the contrary, strontium prefers to be adsorbed better adsorbed by synthetic zeolites [17]. Chemisorption may explain the processes, which are endothermic and spontaneous. Natural zeolites present multilayer adsorption, whereas synthetic ones present monolayer adsorption. Some composites have managed to increase the adsorption without a doubt by a synergic effect. As expected, cesium adsorption is hindered by ammonia, potassium, and sodium and that of strontium by calcium and magnesium.

Ion exchange was regarded as a domain adsorption mechanism of metal ions in solution by zeolite; meanwhile, inner-surface complexation was domain one for aluminosilicate. Ion exchange and inner-surface complexation might be mainly responsible for adsorbing metal ions onto the AlSi/NaY composite. The pore-filling mechanism was a less significant contributor during the adsorption process [43]. The results of competitive adsorption under binary components (Cu^{2+} and Sr^{2+}) and ternary components (Cu^{2+}, Pb^{2+}, and Sr^{2+}) demonstrated the removal efficacy of target metals by the aluminosilicate zeolite, and their composite remarkably decreased. The synthesized AlSi/NaY composite might serve as a promising adsorbent for natural water treatment.

One of the representatives of the aluminosilicates of the zeolite family having a frame structure is the nosean-sulfate form of zeolite $Na_8[AlSiO_4]_6(SO_4)$ with an intermediate frame structure between the well-known zeolites sodalite and cancrinite [44]. The nosean structure is typical for aluminosilicates and consists of alternating SiO_4^{4-} and AlO_4^{5-} tetrahedra, forming a β-frame of four- and six-membered rings, where ion-exchange cations and water are present in the cavities of the frame, including an additional anion SO_4^{2-} [45,46]. These parameters indicate an obvious tendency of nosean to ion-exchange sorption with selectivity for cesium and strontium, similar to various and widely known zeolite forms. However, studies on the use of nosean as a sorbent are very limited in the literature. There are known works on Ca^{2+}, Mg^{2+}, Cu^{2+} sorption [47] and some organic pollutants [48] from aqueous media, and have also been tested for the purification of gas emissions [49]. There are no studies on the synthesis and study of the properties of magnetic composites of nosean, including for the sorption of radionuclides, in the open literature. In this regard, the number of proposed methods for the synthesis of nanostructured composites based on zeolites is limited, and the relationship between the synthesis conditions, physical-chemical characteristics, magnetic and sorption properties has not been sufficiently studied.

The work aimed to synthesize the nanostructured magnetic zeolite nosean in the composition with the magnetite phase (Fe_3O_4) by hydrothermal method. The novelty of study consisted: (i) the development of a new method for the synthesis of the obtained composites, characterized by simplicity of implementation, (ii) the study of the influence of heat treatment conditions during synthesis on the composition, crystalline and porous structure, sorption and magnetic properties of composites, (iii) experimental confirmation of the high efficiency of the obtained magnetic sorbents for the purification of liquid media from cesium and strontium radionuclides.

2. Materials and methods

2.1. Chemicals

The synthesis of nanostructured sorbents based on synthetic nozean zeolite and iron oxide was carried out by the method of joint deposition (Massard method) [50] using a solution of $FeCl_3 \cdot 6H_2O$ and the Mohr salt $Fe(NH_4)_2(SO_4)_2 \cdot 6H_2O$. Monoethylene

glycol was used as a stabilizer of the obtained iron nanoparticles. Zeolite was obtained using sodium silicate $Na_2SiO_3 \cdot 5H_2O$, sodium aluminate $NaAlO_2$. All reagents were supplied by Sigma-Aldrich, 99.9% purity.

2.2. Synthesis of composite

The synthesis of magnetic composites based on zeolite was carried out in two stages: (i) initially, magnetite (Fe_3O_4) nanoparticles were obtained by co-precipitation in an aqueous glycol solution, (ii) then hydrothermal crystallization of aluminosilicate was carried out, according to the following scheme. To a dilute aqueous solution of monoethylene glycol (MEG ratio: water 1:1) with a volume of 120 ml, powders in the amount of 12 mmol $FeCl_3.6H_2O$ and 8.3 mmol $Fe(NH_4)_2(SO_4)_2 \cdot 6H_2O$ were added under heating (80 °C) and constant stirring on a magnetic stirrer. Then 35 ml of a 24% ammonia solution was poured drop by drop and left for 20 min with stirring. 17.2 ml of 2 M $Na_2SiO_3 \cdot 5H_2O$ solution and 52.8 ml of 0.325 M $NaAlO_2$ solution were alternately added to the resulting solution. The resulting solution was left for 30 min with stirring. The temperature of the solution during the entire synthesis was maintained in the range of 75–85 °C. Then it was poured into an autoclave with a volume of 250 ml and kept at temperatures of 90, 120, 150, 180 °C, and a pressure of 90–70.12 kPa, 120–198.48, 150–475.72, 180–1001.9 kPa for 6 h. Then the resulting black precipitate was filtered, washed with distilled water to a neutral filtrate medium, and dried at 90 °C for 4 h.

2.3. Physical-chemical methods

The phases of the obtained samples were identified using X-ray phase analysis (XRD) on an X-ray diffractometer D8 Advance Bruker-AXS (Germany), CuKα radiation, Ni filter, average wavelength (λ) 1.5418 Å, shooting angle range of 10–80°, scanning step of 0.02°, the speed of registration of spectra of 5°C/min. The specific surface area was determined on the ASAP MP 2020 device Micromeritics GmbH (USA) by the method of physical adsorption-desorption of nitrogen at a temperature of 77 K, the data were calculated using the BET method. The analysis of filtrates for the content of cesium and strontium was determined on the atomic absorption spectrophotometer AA-7000 Shimadzu (Japan), the determination error did not exceed 5%. Images of the surface of the samples were obtained using a Carl Zeiss Ultra 55 scanning electron microscope (SEM, Germany), with the prefix for energy-dispersive X-ray microanalysis (EDX) Bruker (Germany). The magnetic characteristics were studied on a vibromagnetometer (VSM) included in the station for measuring the physical properties of matter (PPMS) of the company Quantum Design (USA), as well as on LakeShore 7401 VSM (USA).

2.4. Batch adsorption test

The sorption properties of magnetic composites obtained at different temperatures of hydrothermal synthesis were studied under batch adsorption test use of cesium and strontium stable isotopes. Sorption isotherms were obtained using solutions with different CsCl and $Sr(NO_3)_2$ concentrations, the pH value of the liquid media was 6.0 ± 0.5. The initial concentration of stable cesium and strontium ions in the model solutions was 150 mg/l.

The experiment was carried out according to the following scheme. A 10 mg sorbent sample was placed in an Eppendorf test tube and 10 ml of stable cesium or strontium solution was poured (solid/liquid = 1/1000). A series of test tubes were fixed on a vertical shaker and mixed at rate of 20 rpm. Sorption was carried out within 48 h. After that, the solution was separated from the spent sorbent using a "blue ribbon" filter and the residual content of stable cesium and strontium ions was determined by atomic absorption spectrometry.

The calculation of removal efficiency (RE, %) was carried out according to Eq. (1):

$$RE = \frac{C_0 - C_e}{C_0} \cdot 100\%, \quad (1)$$

where are C_0 – the initial concentrations of Cs^+ and Sr^{2+} ions, mg/l; C_e – equilibrium concentrations of Cs^+ and Sr^{2+} ions, mg/l.

The sorption mechanism was evaluated based on the Cs^+ and Sr^{2+} sorption isotherms, which represent the dependence of the amount of the adsorbed substance on the concentration of the solution at a constant temperature. When describing the sorption isotherms, well-known sorption models at the solid/liquid boundary were used.

Freundlich equation:

$$q = K_F \cdot C^m, \quad (2)$$

where are C – the equilibrium Cs^+ and Sr^{2+} concentrations (mg/l); K_F – the Freundlich constant, which characterizes the relative adsorption capacity and represents the value of adsorption at an equilibrium concentration equal to one; m – an indicator of the heterogeneity of exchange centers, which characterizes the change in the heat of adsorption depending on the degree of their filling.

Langmuir equation:

$$q = q_{max} \frac{K_L \cdot C}{1 + K_L \cdot C} \quad (3)$$

where are q_{max} – the value of the maximum sorption (mg/g); C – the equilibrium Cs^+ and Sr^{2+} concentrations (mg/l); K_L – the constant of the adsorption equilibrium, characterizing the energy of the adsorbent-adsorbate bond.

Langmuir-Freundlich equation:

$$q = q_{max} \frac{K_{LF} \cdot C^m}{1 + K_{LF} \cdot C^m}, \quad (4)$$

where are q_{max} – the value of the maximum sorption (mg/g); C – the equilibrium Cs^+ and Sr^{2+} concentrations (mg/l); K_{LF} – the constant of the adsorption equilibrium, characterizing the energy of the adsorbent-adsorbate bond; m – an indicator of the heterogeneity of exchange centers, which characterizes the change in the heat of adsorption depending on the degree of their filling. The approximation of the experimental data by these equations in a nonlinear form was carried out using the SciDavis program.

2.5. Determination of sorption characteristics to radionuclides ^{137}Cs and ^{90}Sr

The sorption characteristics of the samples were determined by the example of the sorption of trace amounts of ^{137}Cs and ^{90}Sr radionuclides. The experiments were carried out under static conditions by continuously mixing a sample of an air-dry sorbent weighing about 0.1 g, weighed with an accuracy of 0.0001 g from 20 cm^3 of solution for 24 h. Then the mixture was filtered through a paper filter "white ribbon," and the specific activity of ^{137}Cs in the filtrate was determined by a direct radiometric method using a spectrometric complex SKS-50 M (Green Star Technologies, Moscow). Based on the analysis results, the values of the distribution coefficient (Kd) of the corresponding radionuclide were calculated using the formula:

$$K_d = \frac{A_0 - A_p}{A_p} \times \frac{V_p}{m_c} \quad (5)$$

where, A_o, A_p – respectively, the specific activity of the ^{137}Cs or ^{90}Sr radionuclide in the initial solution and in the filtrate, Bq/dm^3;

V_p – volume of the liquid phase, cm^3;

m_c – sorbent mass, g;

In the study of **^{137}Cs**, the following solutions were used as the liquid phase:

- 0,1 mol/dm^3 solution $NaNO_3$, pH = 6,0;
- 1,0 mol/dm^3 solution $NaNO_3$, pH = 6,0;
- seawater sampled in the Sevastopol Bay of the Black Sea (sampling date - November 22, 2019). The salinity of water - 21.2 g/l, pH – 7.8.

Before starting the experiments, indicator amounts of ^{137}Cs radionuclide in about 105 Bq/dm^3 were added to the solution and kept for three days at room temperature to achieve equilibrium of various ionic radioactive forms the solution components.

In the study of **^{90}Sr**, the following solutions were used as the liquid phase:

- 0,01 mol/dm^3 solution $CaCl_2$, pH = 6,0;
- 0,1 mol/dm^3 solution $NaNO_3$, pH = 6,0;
- seawater sampled in the Sevastopol Bay of the Black Sea (sampling date - November 22, 2019). The salinity of water - 21.2 g/l, pH - 7.8.

Before starting the experiments, indicator amounts of ^{90}Sr radionuclide in an amount of about 105 Bq/dm^3 were added to the solution and kept for at least three days at room temperature to achieve equilibrium ionic and radioactive forms of the solution components.

A beta spectrometric channel determined the specific activity of ^{90}Sr in solutions from the total beta activity on an SKS-50 M spectrometric complex (Green Star Technologies, Russia). Samples containing ^{90}Sr were kept for at least 14 days before measurement to establish the radioactive equilibrium of the ^{90}Sr–^{90}Y vapor.

During the sorption of ^{90}Sr from solutions of calcium salts, in addition to the (K_d) values of ^{90}Sr, the values of the static exchange capacity (SEC) for calcium and the separation coefficient of the Sr/Ca pair ($D_{Sr/Ca}$) were calculated according to formulas 6 and 7, respectively:

$$SEC = (C_o - C_p) \times V_p/m_c \quad (6)$$

$$D_{Sr/Ca} = (K_d \times C_p)/SEC \quad (7)$$

where

Co, Cp - respectively, the concentration of Ca^{2+} ions in the initial solution and in the filtrate, mmol/cm^3;

K_d - distribution ratio ^{90}Sr, cm^3/g.

The concentration of calcium ions in solutions was determined by the volumetric complexometric method.

3. Results and discussions

During hydrothermal synthesis, magnetic composite powders were obtained at different temperatures, the phase composition of which is shown in Fig. 1. The main crystalline phase of all samples is magnetite (Fe_3O_4). The crystalline phase of the aluminosilicate appears on the X-ray image only for the sample obtained at 180 °C (Fig. 1a). This phase was identified as the carbonate form of the nozean frame aluminosilicate $Na_8[AlSiO_4]_6(CO_3)$ [51]. A detailed comparison of the X-ray diffraction results for the sample obtained at 180 °C with the diffractograms of the reference crystal phases shows that the main diffraction maxima of 2θ 13.9°, 24.2° and 34.5° correspond to $Na_8[AlSiO_4]_6(CO_3)$, along with the rest, which is comparable to Fe_3O_4 diffraction pattern (Fig. 1b).

To visualize the crystal structures of the obtained aluminosilicate compounds, their structural 3D models were constructed (Fig. 2) using the VESTA software (Letia and Groza, 2009). The parameters of the unit cell of the synthesized carbonate form of nosean coincide with the calculated ones and correspond to the cubic form a = b = c = 9.001 Å, while for the sulfate form the calculated parameters correspond to the cubic form a = b = c = 9.084 Å. According to the obtained models, it can be seen that the packing density of atoms in the crystal lattice of the sulfate form is slightly higher compared to the carbonate one.

According to the SEM data (Fig. 3), the structure of the obtained samples of magnetic composites was represented by nanoscale (significantly less than 50 nm) spherical particles agglomerated

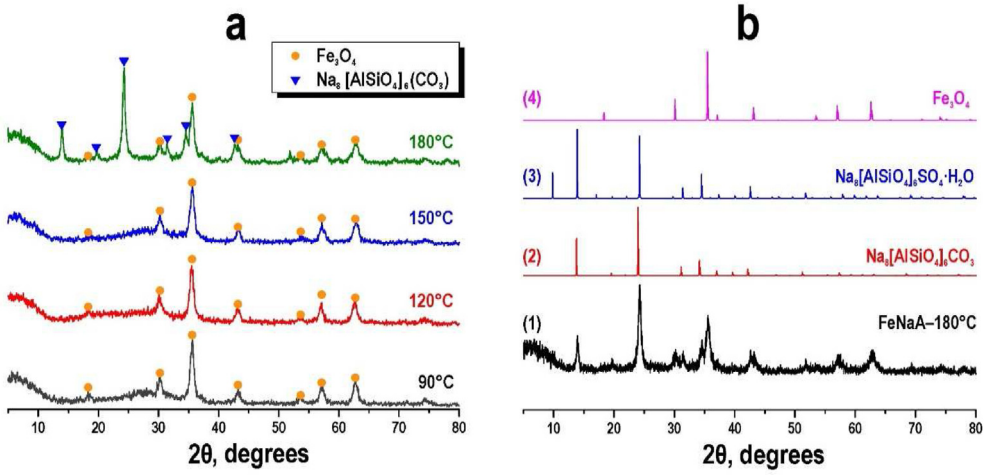

Fig. 1. Diffractograms of nanostructured magnetic composites: (a) samples obtained at different temperatures of hydrothermal synthesis; (b) comparison of the experimental sample obtained at 180 °C with the corresponding reference structures.

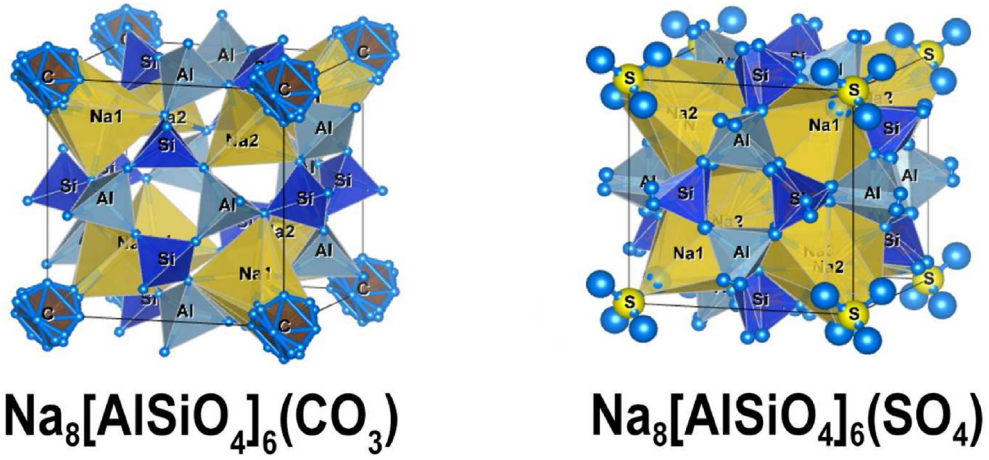

Fig. 2. Model images of the crystal structures of the carbonate and sulfate forms of the frame alumosilicate nosean.

with each other. The results of the study showed that the size of these nanoparticles increased with an increase in the temperature of hydrothermal synthesis. The surface morphology of the magnetic zeolite sample obtained at 180 °C differed significantly (Fig. 3d, d*). The particles were agglomerated into large spherical formations, the surface of which was structured by crystallites with smooth faces. This is probably due to the formation of a crystalline aluminosilicate from the amorphous phase, as was shown in the X-ray diffraction analysis for this sample (Fig. 1).

According to the data of the elemental analysis carried out by X-ray fluorescence and EDX methods (Table 1), it was found that the quantitative ratio of Al_2O_3/SiO_2 varied within 1.4–1.9, which corresponded to zeolite A-type structure. The ratio of magnetite and aluminosilicate was maintained within 1:3.

As a result of grain growth, the number of contacts between particles increased, and larger agglomerates were formed, as was shown in the SEM images (Fig. 3a-c*). As a result, this led to a decrease in the BET surface area from 40 to 18.3 m^2/g, which was determined by the results of nitrogen adsorption-desorption (Fig. 4a–d). It was shown that the isotherms of low-temperature nitrogen adsorption-desorption for these samples obtained within 150 °C had an identical character and belong to type IV according to the IUPAC classification, characteristic of mesoporous solids (Fig. 4a–c). The hysteresis loops shape was of H1 type with a sharp increase in the sorption capacity in the region of high relative pressures $p/p_0 \rightarrow 0.95–0.99$, which indicates the presence of slit-like shapes in composites structure. This was due to the similar morphology and type of porous structure of these samples, which was confirmed by the identical size range of meso- and macropores, which was determined by the DFT method (Fig. 4a* - c*).

The sample synthesized at 180 °C had an obvious difference, the value of A_{BET} increased to 54.8 m^2/g and the transition of hysteresis loop shape of the nitrogen adsorption-desorption isotherm from the H1 to H2 type indicated the formation of cylindrical mesopores in the sample (Fig. 4d). This was confirmed by DFT method calculation, where the pore size distribution graph showed that mesopores with a size in the range of 5–32 nm were formed in the sample (Fig. 4d*). Such a difference in this sample was due to a change in its general structure and surface morphology (a change in the shape of particles from spherical to crystalline; their packaging and spatial agglomeration, etc.), as was shown above in the SEM image (Fig. 3d, d*).

Fig. 5 shows the Cs^+ sorption isotherms at pH 6.0 ± 0.5, as well as the curves obtained by approximating the experimental data with the Langmuir, Freundlich, and Langmuir-Freundlich models. It was shown that with an increase in the temperature of hydrothermal synthesis, the values of the maximum sorption (q_{max}) decreased, which indicates a decrease in the number and availability of sorption centers for ion exchange. This was probably due to their growth and agglomeration, as was shown on SEM images for samples obtained in the range of 90–150 °C (Fig. 3a-c*), as well as a decrease in the specific surface area and pore volume (Fig. 4 a, a*-c, c*). The sample obtained at 180 °C had the lowest sorption capacity, which was characterized by the highest value of t BET surface area (Fig. 4), which was mainly due to a change in the composition of nosean aluminosilicate $Na_8[AlSiO_4]_6(CO_3)$ crystalline phase (Fig. 1, Table 1).

Table 2 showed the corresponding values of the adsorption equilibrium constants (K_L) and the maximum sorption (q_{max}). Based on the high values of the correlation coefficients (R^2) and the correspondence of the calculated and experimental values of the sorption capacity. It can be concluded that the experimental data were reliably described by the Langmuir equation. This indicated the occurrence of predominantly monomolecular adsorption, which was characteristic of the ion-exchange sorption mechanism. It was shown that the sample obtained at 90 °C had the greatest sorption capacity, which was probably due to its chemical composition (Table 1) and the largest number of active ion exchange (sorption) centers on the magnetic composite surface.

According to the C. H. Giles classification [52], the isotherms in Fig. 5a can be attributed to the C-type, which is characterized by a linear initial section, which corresponds to the preservation of the number of adsorbed centers in a wide range of cesium concentrations, up to the maximum possible adsorption of the adsorbent from the solution. At the same time, the conditions for obtaining type-C isotherms were the presence of “flexible” layers or regions with different degrees of crystallinity in the porous sorbent; the high affinity of the adsorbing substance (cesium ions) to the sorbent; the high penetrating ability of the adsorbent to the structural geometry of the sorption material.

3.1. Determination of sorption characteristics to the ^{137}Cs radionuclide

To obtain comparative characteristics of the studied samples under similar conditions, we carried out the sorption of cesium and

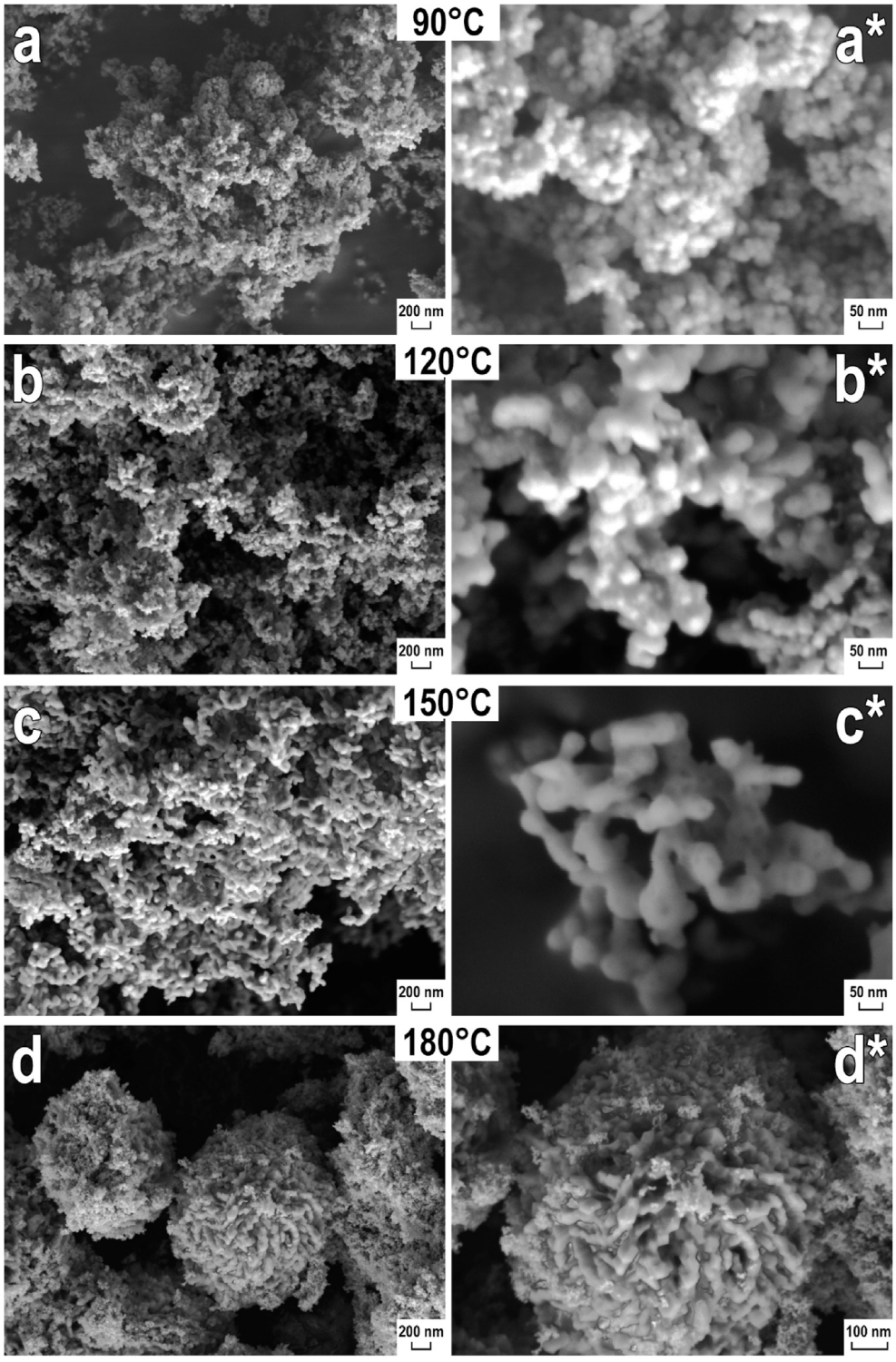

Fig. 3. SEM images of nanostructured magnetic composites obtained at different temperatures of hydrothermal synthesis, a,a* - NaFeA-90, b,b* - NaFeA-120, c,c* - NaFeA-150, d,d* - NaFeA-180.

strontium radionuclides on the sorbents listed in (Table 3).

3.2. Determination of sorption characteristics for ^{90}Sr radionuclide

To obtain comparative characteristics of the studied samples under similar conditions, ^{90}Sr was sorbed on the presented sorbents. The values of the distribution coefficients (K_d) of ^{90}Sr on various sorbents upon sorption from model solutions of the above composition are given in Table 5.

Presented in Table 5, the results show that in a 0.1 mol/dm^3 $NaNO_3$ solution, the studied NaFeA sorbent has high sorption characteristics with respect to ^{90}Sr. However, in the presence of calcium ions and seawater, it is significantly inferior to known sorption materials – titanium phosphate, silicotitanate and MDM

Table 1
The content of oxide phases in magnetic composites obtained at various temperatures of hydrothermal synthesis.

$T_{synthesis}$, °C	X-ray fluorescence analysis, wt. %				EDX analysis, wt. %			
	Fe_3O_4	Na_2O	SiO_2	Al_2O_3	Fe_3O_4	Na_2O	SiO_2	Al_2O_3
90	25.9	13.3	36.0	24.8	22.5	15.8	39.9	21.8
120	25.0	15.7	34.8	24.6	24.3	15.6	38.7	21.4
150	24.6	15.7	35.1	24.6	25.5	15.5	37.8	21.2
180	23.0	18.9	34.8	23.3	24.4	18.7	36.3	20.5

sorbents.

Magnetic zeolite NaFeA has a high calcium capacity (3.57 mmol/g). However, the selectivity to strontium in the presence of calcium ions is low and significantly inferior to almost all known studied sorbents, as shown in Table 6.

Fig. 6 shows Sr^{2+} ions sorption isotherms at pH 6 ± 1, as well as curves obtained by approximating experimental data with the Langmuir, Freundlich, and Langmuir-Freundlich models.

Table 7 showed the calculated parameters for these models. The isotherms for the samples synthesized at 90 and 120 °C had an H-type [52] at which there was a steeply ascending section in the region of low concentrations (Fig. 6a and b). This indicated high affinity of sorbent to the Sr^{2+} ions and a high adsorption on the sorbent surface. Isotherms of this type are the result of an exchange between the functional groups of the sorbent and Sr^{2+} ions formed during dissociation of the adsorbent in solution. For samples synthesized at 150 and 180 °C, the isotherms were of the L-type, which is characterized by a curved initial section relative to the concentration axis (Fig. 6c and d). Since with an increase in the proportion of adsorption sites occupied by Sr^{2+} ions, it is more difficult to find a vacant place, especially if the crystallites tend to form large agglomerates, as shown in the SEM (Fig. 3c*-d*), the formation of which in solution was due to increased intermolecular interaction.

Table 7 shows the calculated equation parameters after experimental data approximation. Thus, the strontium ions sorption proceeded by a monomolecular mechanism, mainly due to ion exchange, which is confirmed by a reliable description of the experimental data by the Langmuir model. At the same time, with an increase in the temperature of hydrothermal synthesis, the maximum sorption value (q_{max}) decreased, which is consistent with changes in the specific surface area (Fig. 4), the chemical composition (Table 1), and the surface morphology of the samples (Fig. 3). The sample synthesized at 90 °C had the greatest sorption capacity, which, as in the case of Cs^+ sorption, was associated with the largest number of ion-exchange centers on the magnetic composite surface. The same results were revealed by Kouznetsova et al. [43] for studying Sr^{2+}, Cu^{2+}, and Pb^{2+} ions adsorption on novel mesoporous aluminosilicate/zeolite composites. It was shown that ion-exchange process was regarded as a domain adsorption mechanism of metal ions in solution by zeolite. Meanwhile, inner-surface complexation was domain one for aluminosilicate.

The study of the magnetic characteristics of nanostructured composites included the determination of the specific magnetization in a state close to saturation (M), as well as the coercive force (H_c). Additionally, the temperature dependence of the specific saturation magnetization of the samples was measured to study the influence of the temperature conditions of their synthesis on the magnetic parameters of the magnetite phase, which is part of the samples and determines their general magnetic properties.

Fig. 7 shows the dependences of the specific magnetization of the studied samples on the applied field strength (H). It was established that for all the studied samples there is a complete absence of hysteresis (H_c and residual magnetization Mr are equal to 0). This behavior was possible for magnetite particles in the superparamagnetic state [53]. For magnetite, the critical volume of nanoparticles in the superparamagnetic state was equal to:

$$V_{sp} = \frac{25 k_B T}{K_u} \quad (8)$$

where are k_B is the Boltzmann constant, T is the sample temperature at measurement (T), K_u is the magnetic anisotropy ($K_u = -1{,}1 \times 10^5$ erg/cm^3) [54].

The calculated critical diameter of magnetite nanoparticles was equal to $D_{sp} = 26$ nm. The magnetization behavior of an ensemble of nanoparticles in a magnetic field was well described by the Langevin function, which confirms the presence of a superparamagnetic state:

$$M_i = M\left(\coth\left(\frac{mH}{k_B T}\right) - \frac{k_B T}{mH}\right) \quad (9)$$

where are $m = \frac{M\pi D^3}{6}$ is the magnetic moment of each nanoparticle, D is the diameter of the nanoparticle [54].

The average diameter of the nanoparticles calculated from the approximation for all samples was 27.9 ± 1.5 nm, which is in good agreement with the D_{sp}. It is important to note that the size of Fe_3O_4 nanoparticles did not change with an increase in the temperature of hydrothermal synthesis.

The unambiguous relationship between the specific saturation magnetization and the applied field strength for the main magnetization curve, for the curve M(H) with an increase and decrease in the conditionally positive and negative H values allowed to limit ourselves to two branches of the dependence M(H) (Fig. 7). The calculated (theoretical) value of the specific magnetization of iron at its content for 12–15 wt % in the composition of the magnetite phase was 17–19 emu/g. For comparison, specific magnetization of magnetite saturation was 92.4 emu/g, and the weight content of iron in its composition was 72 wt%. Thus, the experimentally obtained value of the specific magnetization of saturation fully corresponded to the amount of iron in the magnetite phase composition. The experimentally measured values of the specific saturation magnetization completely coincided with the calculated value (Fig. 7).

Fig. 8 shows the dependences of the specific saturation magnetization of the studied samples on the heating temperature. It was determined that the Curie temperature for all the studied samples was 580 °C. Thus, the temperature conditions of hydrothermal synthesis studied in the range of 90–180 °C did not affect the composition and structure of the magnetic phase, and the oxidation of magnetite did not occur.

The results of magnetic studies showed that the coercive force was close to zero, so the synthesized nanostructured composite sorbents belong to soft magnetic materials with a relatively high specific saturation magnetization. In this regard, firstly, the particles of this sorbent in the absence of a magnetic field will not have a dipole interaction, which will exclude their agglomeration when dispersed in purified solutions. Secondly, when such a sorbent was exposed to a constant 2000–3000 Oe, its high efficiency of magnetic separation will be achieved.

4. Conclusions

Magnetic nanostructured sorbents based on composites of zeolite nosean and magnetite were obtained by hydrothermal synthesis. It was established that in the samples obtained during hydrothermal treatment in the range of 90–150 °C, only the

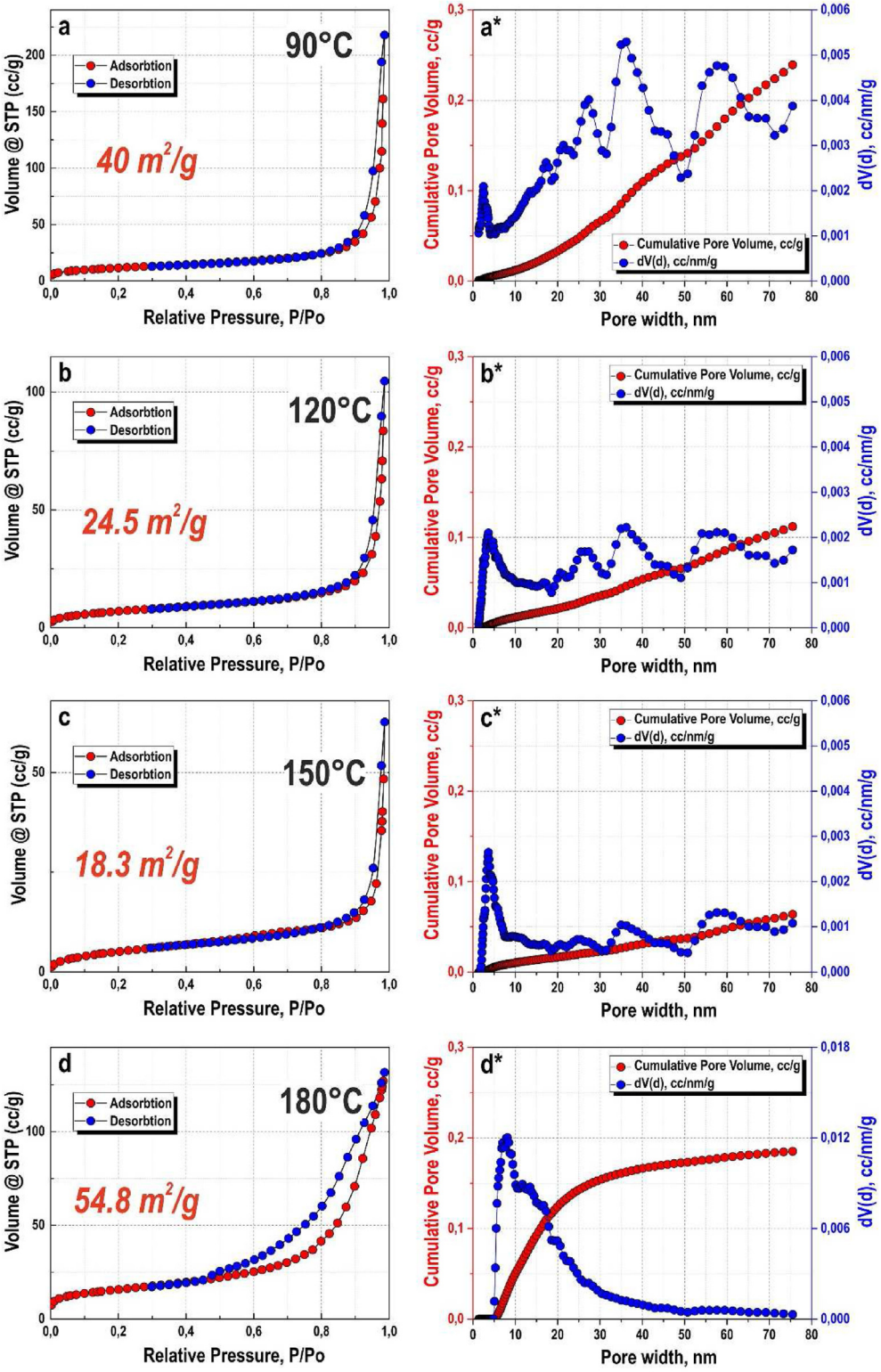

Fig. 4. Isotherms of low-temperature nitrogen adsorption-desorption(a-d) and pore size distribution(a*-d*) calculated by the DFT method of nanostructured magnetic composites obtained at different temperatures of hydrothermal synthesis.

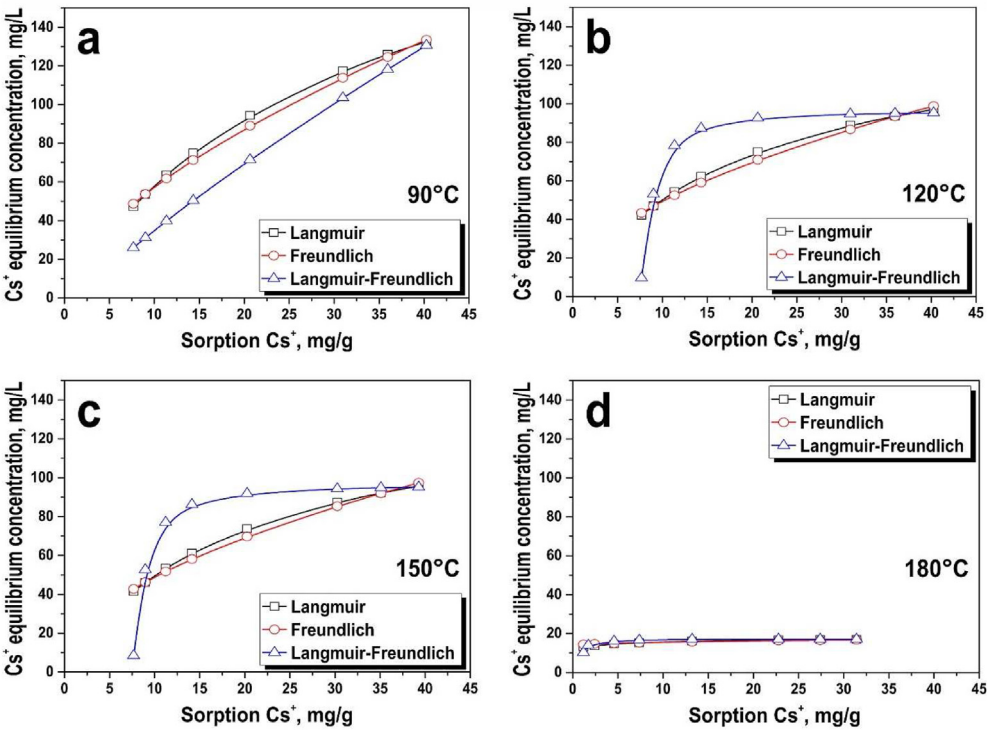

Fig. 5. Isotherms of cesium sorption by nanostructured magnetic composites obtained at different temperatures of hydrothermal synthesis and approximation isotherms based on Langmuir, Freundlich, and Langmuir-Freundlich models.

Table 2
Calculated parameters of the Langmuir, Freundlich, and Langmuir-Freundlich models for Cs^+ sorption isotherms.

Model	Parameters	$T_{synthesis}$, °C			
		90	120	150	180
Langmuir	q_{max}	229.6	139.9	139.9	18.18
	K_L	0.08	0.05	0.05	2.61
	R^2	0.92	0.99	0.99	0.74
Freundlich	K_F	24.20	15.73	15.29	14.46
	n	0.60	0.49	0.50	0.08
	R^2	0.88	0.99	0.99	0.73
Langmuir-Freundlich	q_{max}	192.41	96.35	96.67	17.03
	K_{L-F}	0.95	0.95	1.02	0.68
	R^2	0.99	0.83	0.84	0.49

Table 3
Characteristics of the materials used for the sorption of cesium and strontium radionuclides.

Sorbent	Manufacturer	Sorbent composition	Particle size, mm	Technical conditions
NaA	Ishimbay Chemical Catalyst Plant, Republic of Bashkiria, Russia;	Sodium form of type A zeolite	0.2–0.5	2163-003-15285215-2006.
Clinoptilolite	Deposits "Sokirnitsa", Ukraine	Zeolite	0.2–0.5	14.5-00292540.001-2001
Termoxid 35	JSC "TERMOXID"Co (Zarechny, Sverdlovsk region)	Zirconium Hydroxide Nickel potassium ferrocyanide;	0.4–1.5	2641-019-57983206-2012
Termoxid 3A	JSC "TERMOXID"Co (Zarechny, Sverdlovsk region)	Sorbent based on hydrated titanium and zirconium dioxides	0.4–1	2641-004-12342266-2004
FT-1	ICTREMS KSC RAS, Apatity;	Titanium phosphate	0.3–0.5	–
TC-1	ICTREMS KSC RAS, Apatity;	Sodium potassium titanosilicate	0.3–0.5	–
FNC-10	SPE Ektos-Atom, JSC (Moscow)	Nickel potassium ferrocyanide	0.2–0.5	2641-012-57989206-2012
MDM	Industrial batch, manufacturer - IPCE RAS	Sorbent based on modified manganese dioxide	0.2–0.5	2641-001-51255813-2007

The values of the distribution coefficients (K_d) of ^{137}Cs on various sorbents during sorption from model solutions of the above composition are given in (Table 4).

Table 4
Values of the distribution coefficient (K_d) of ^{137}Cs on various sorbents during sorption from model solutions.

Sorbent	K_d values of ^{137}Cs, cm^3/g in solution:		
	0,1 mmol/dm^3 $NaNO_3$	1,0 mmol/dm^3 $NaNO_3$	Sea water
NaFeA	2.5×10^3	0.2×10^3	1.7×10^3
NaA	8.9×10^3	0.7×10^3	0.2×10^3
Clinoptilolite	1.6×10^3	0.1×10^3	1.5×10^3
FT-1	7.3×10^3	0.8×10^3	8.8×10^3
TC-1	5.7×10^4	2.9×10^4	$1,8 \times 10^4$
FNC-10	8.4×10^4	7.3×10^4	$1,1 \times 10^4$
Termoxid 35	1.2×10^5	8.1×10^4	$3,1 \times 10^4$

The results presented in the table show that in terms of sorption characteristics with respect to ^{137}Cs, the NaFeA sample is superior to NaA and Clinoptilolite, only in seawater. Regarding absolute K_d values, ^{137}Cs NaFeA in all studied media is inferior to almost all studied sorbents.

Table 5
Values of the distribution coefficient (K_d) of ^{90}Sr on various sorbents during sorption from model solutions.

Sorbent	Kd values of ^{90}Sr, cm^3/g in solution		
	0,01 mmol/dm^3 $CaCl_2$	0,1 mmol/dm^3 $NaNO_3$	Sea water
NaFeA	1.5×10^3	$1,1 \times 10^4$	0.2×10^3
NaA	0.3×10^3	$8,5 \times 10^4$	–
Clinoptilolite	0.3×10^2	0.3×10^2	˂ 10
Termoxid 3K	0.2×10^3	$3,5 \times 10^4$	0.5×10^3
MDM	5.3×10^3	$4,0 \times 10^4$	0.6×10^3
FT-1	$4,6 \times 10^4$	$5,1 \times 10^4$	4.7×10^3
TC-1	$3,5 \times 10^4$	$4,1 \times 10^5$	7.3×10^3

magnetite crystalline phase was identified, with an increase in the treatment temperature to 180 °C, an impurity of the crystalline zeolite nosean was formed. All samples were characterized by a mesoporous structure with a specific surface area of 18.3–54.8 m^2/g, slit-like and cylindrical pores, for samples obtained at 90–150 and 180 °C, respectively. According to the sorption capacity of stable cesium and strontium ions, the samples were arranged in the following order 90 °C > 120 °C ≈ 150 °C > > 180 °C. The sorption isotherms of cesium and strontium ions were reliably described by the Langmuir monomolecular adsorption equation, which confirmed the ion-exchange sorption mechanism. The maximum sorption capacity to cesium and strontium ions of 229.6 and

Table 6
Values of the static exchange capacity (SEC) for Ca^{2+}, the distribution coefficient (K_d) of ^{90}Sr and the separation coefficient of the Sr/Ca pair ($D_{Sr/Ca}$) on various sorbent samples (solution 0.01 mol/dm^3 $CaCl_2$, pH = 6.0).

Sorbent	SEC for Ca^{2+}, mmol/g	K_d ^{90}Sr, cm^3/g	$D_{Sr/Ca}$
NaFeA	3,57	1.5×10^3	2,1
Termoxid 3K	0,23	0.2×10^3	8,9
FT-1	1,78	$4,6 \times 10^4$	61
TC-1	1,61	$3,5 \times 10^4$	72
MDM	0,83	$5,3 \times 10^3$	37

Table 7
Calculated parameters of the Langmuir, Freundlich, and Langmuir-Freundlich models for Sr^{2+} sorption isotherms.

Model	Parameters	$T_{synthesis}$, °C			
		90	120	150	180
Langmuir	q_{max}	105.1	104.1	27.86	25.87
	K_L	0.75	0.77	1.55	1.73
	R^2	0.93	0.92	0.90	0.98
Freundlich	K_F	41.32	41.53	15.10	14.78
	n	0.29	0.29	0.17	0.13
	R^2	0.90	0.90	0.87	0.91
Langmuir-Freundlich	q_{max}	92.41	96.35	28.10	27.70
	K_{L-F}	0.20	0.95	0.76	0.54
	R^2	0.92	0.93	0.92	0.90

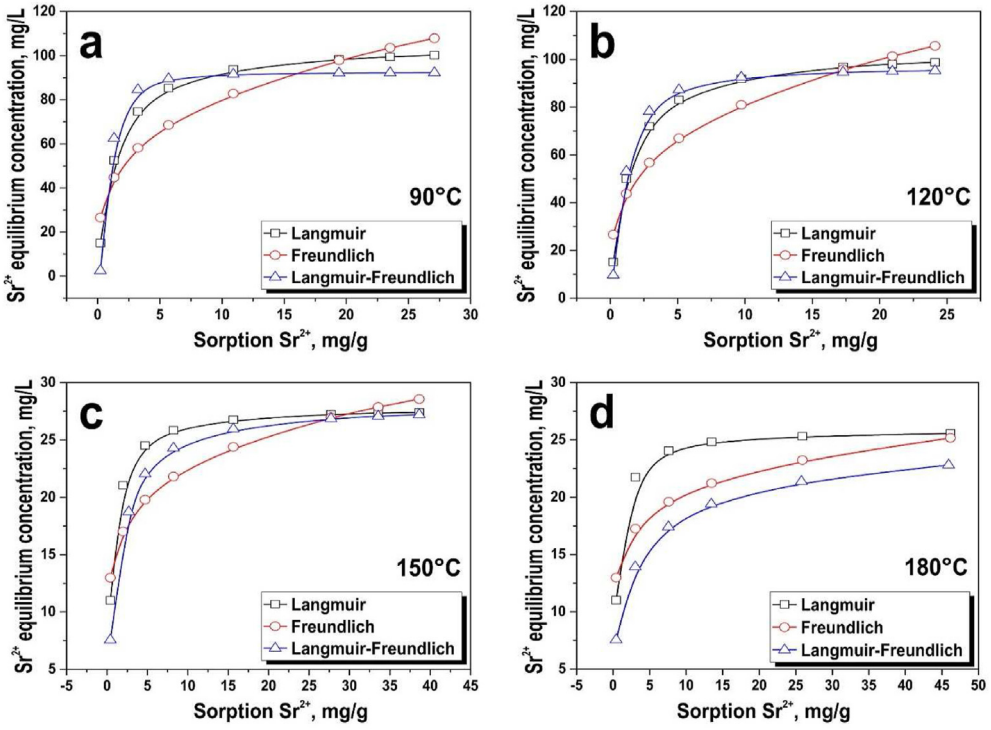

Fig. 6. Isotherms of strontium sorption by nanostructured magnetic composites obtained at different temperatures of hydrothermal synthesis and approximation isotherms based on Langmuir, Freundlich, and Langmuir-Freundlich models.

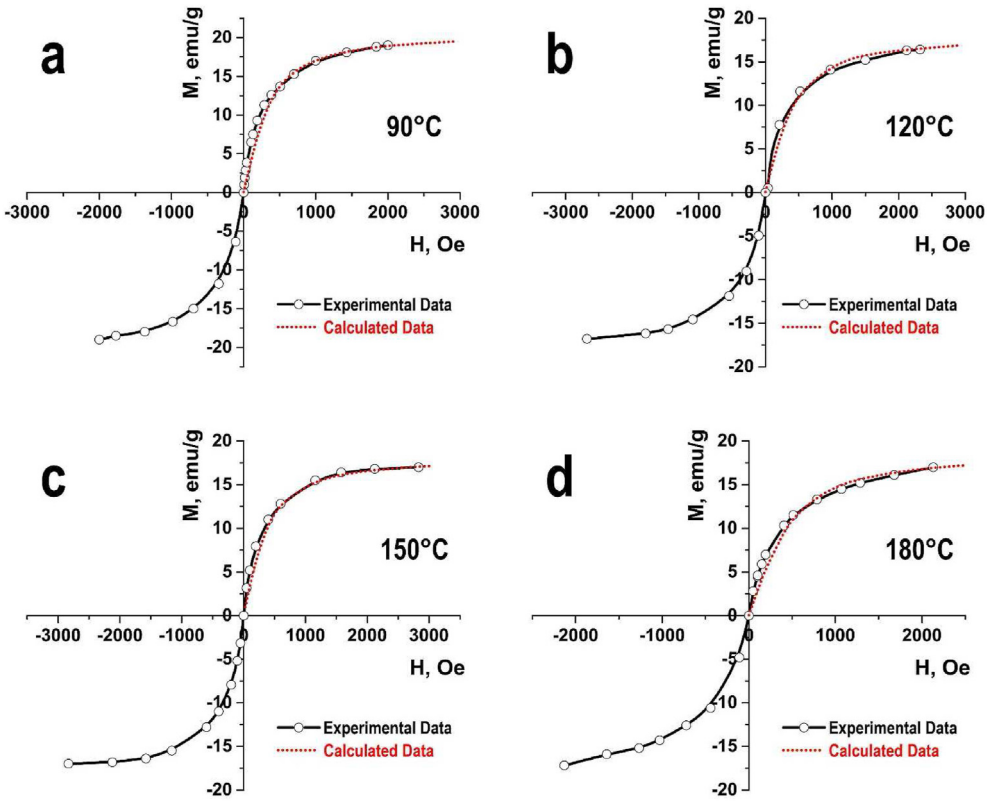

Fig. 7. The dependence of the specific magnetization on the applied field strength for nanostructured magnetic composites obtained at different temperatures of hydrothermal synthesis. The data was approximated by the Langevin function.

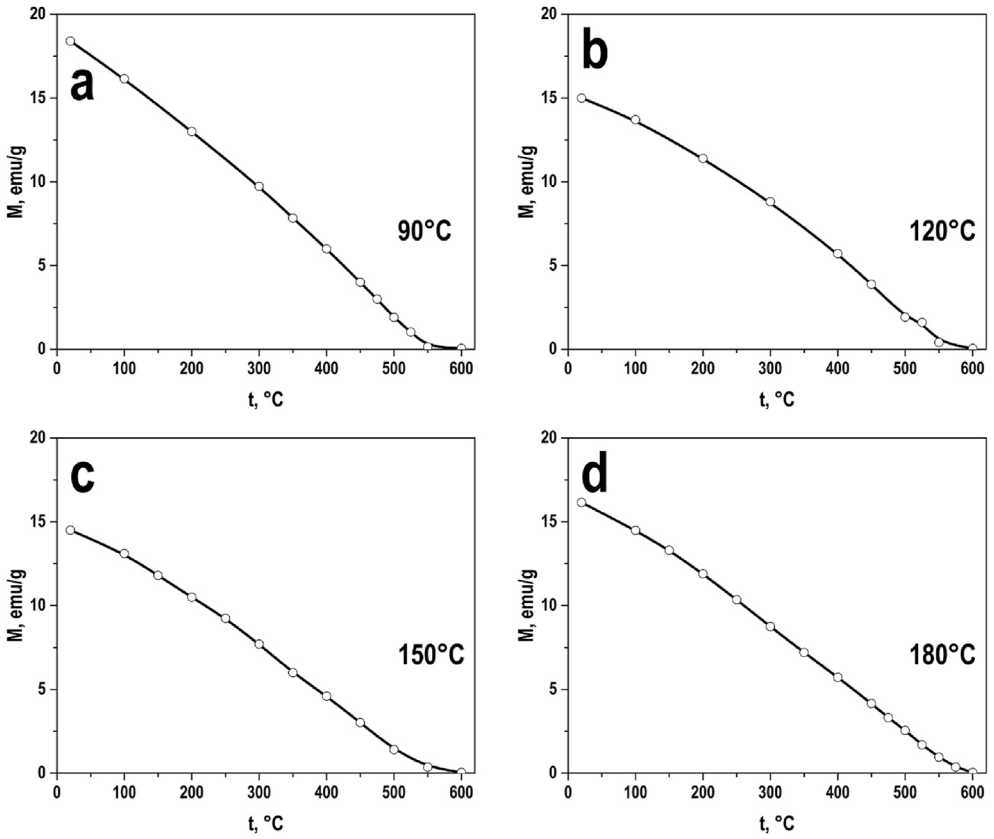

Fig. 8. Dependence of the specific magnetization on the heating temperature of nanostructured magnetic composites obtained at different temperatures of hydrothermal synthesis.

105.1 mg/g was achieved for a sample obtained at 90 °C.

The sorption characteristics of this material with respect to ^{137}Cs and ^{90}Sr radionuclides are superior to sorption materials of a similar type (NaA and clinoptilolite) only in seawater, where the (K_d) value for cesium can reach 1.7×10^3 ml/g, which indicates that they are promising for use in purification of seawater from radioactive cesium. The measured magnetic characteristics of the obtained composites indicated the successful magnetic modification of the nozean zeolite with magnetite and the prospects for the use of a magnetic field during the separation of spent sorbents.

Declaration of competing interest

The authors declare that they have no known competing financial interests or personal relationships that could have appeared to influence the work reported in this paper.

Acknowledgments

The authors are grateful to the staff of the Laboratory of X-ray Diffraction Analysis of the Institute of Chemistry of the Far Eastern Branch of the Russian Academy of Sciences, Ph.D. Gerasimenko A.V. and Ph.D. Shlyk D.H. for conducting X-ray phase analysis of four experimental samples (providing experimental data) and also are grateful to head of laboratory of chromatography of radioactive elements of the Frumkin Institute of Physical chemistry and Electrochemistry Russian Academy of Sciences, Dr.Sci. Milyutin V.V. for conducting of radionuclides sorption analysis.

The investigation was carried out with the financial support of the State Assignment of the Ministry of Science and Higher Education of the Russian Federation topic No. 00657-2020-0006 (Papynov E.K. acknowledges). The assessment of sorption properties was carried out with the financial support of the RFBR, project No. 19-03-00119. The measurement and analysis of the magnetic properties of the samples were carried out with the support of the Russian Science Foundation, project No. 19-72-20071.

The equipment of the joint Center for collective Use, the interdisciplinary center in the field of nanotechnology and new functional materials of the FEFU and the laboratory of magnetism, and the laboratory of film technologies of the FEFU were used in the work. (Far Eastern Federal University, FEFU, Vladivostok, Russia). X-ray phase analysis of four samples was carried out on the equipment of the Far Eastern Center for Structural Research (Institute of Chemistry of the FEB RAS, Vladivostok, Russia).

References

[1] D. Alby, C. Charnay, M. Heran, B. Prelot, J. Zajac, Recent developments in nanostructured inorganic materials for sorption of cesium and strontium: synthesis and shaping, sorption capacity, mechanisms, and selectivity—a review, J. Hazard Mater. 344 (2018) 511–530, https://doi.org/10.1016/j.jhazmat.2017.10.047.

[2] Ö. Arar, Application of sorption process for the removal of radioactive elements, in: A. Núñez-Delgado (Ed.), Sorbents Mater. Control. Environ. Pollut., Elsevier, 2021, pp. 495–512, https://doi.org/10.1016/B978-0-12-820042-1.00020-1.

[3] P.S. Gordienko, I.A. Shabalin, S.B. Yarusova, S.B. Bulanova, V.G. Kuryavyi, V.V. Zheleznov, S.N. Somova, I.G. Zhevtun, Sorption of strontium ions on barium silicates from solutions of complex salt composition, Russ. J. Inorg. Chem. 64 (2019) 1579–1586, https://doi.org/10.1134/S0036023619120052.

[4] V.A. Avramenko, A.M. Egorin, E.K. Papynov, T.A. Sokol'nitskaya, I.G. Tananaev, V.I. Sergienko, Processes for treatment of liquid radioactive waste containing seawater, Radiochemistry 59 (2017), https://doi.org/10.1134/S1066362217040142.

[5] B. Collum, Nuclear fuel cycle, in: Nucl. Facil., Elsevier Ltd., 2017, pp. 1–44, https://doi.org/10.1016/B978-0-08-101938-2.00001-5.

[6] I. Obodovskiy, Radionuclide sources of ionizing radiation, in: Radiat. Fundam. Appl. Risks, Saf., Elsevier, 2019, pp. 259–273, https://doi.org/10.1016/b978-0-444-63979-0.00017-3.

[7] O. Evrard, J.P. Laceby, H. Lepage, Y. Onda, O. Cerdan, S. Ayrault, Radiocesium transfer from hillslopes to the Pacific ocean after the Fukushima nuclear power plant accident: a review, J. Environ. Radioact. 148 (2015) 92–110, https://doi.org/10.1016/j.jenvrad.2015.06.018.

[8] V.V. Levenets, A.Y. Lonin, O.P. Omelnik, A.O. Shchur, Comparison the sorption properties of clinoptilolite and synthetic zeolite during sorption strontium from the water solutions in static conditions: sorption and quantitative determination of strontium by the method PIXE, J. Environ. Chem. Eng. 4 (2016) 3961–3966, https://doi.org/10.1016/j.jece.2016.09.011.

[9] E. Han, Y.G. Kim, H.M. Yang, I.H. Yoon, M. Choi, Synergy between zeolite framework and encapsulated sulfur for enhanced ion-exchange selectivity to radioactive cesium, Chem. Mater. 30 (2018) 5777–5785, https://doi.org/10.1021/acs.chemmater.8b02782.

[10] T.A. Vereshchagina, S.N. Vereshchagin, N.N. Shishkina, N.G. Vasilieva, L.A. Solovyov, A.G. Anshits, Microsphere zeolite materials derived from coal fly ash cenospheres as precursors to mineral-like aluminosilicate hosts for 135,137Cs and 90Sr, J. Nucl. Mater. 437 (2013) 11–18, https://doi.org/10.1016/j.jnucmat.2013.01.343.

[11] S. Smeets, X. Zou, Zeolite structures, in: J. Cejka, H. Bekkum (Eds.), Stud. Surf. Sci. Catal., Elsevier Ltd., 2005, pp. 37–72, https://doi.org/10.1039/9781788010610-00037.

[12] G.D. Gatta, P. Lotti, Systematics, crystal structures, and occurrences of zeolites, in: M. Mercurio, B. Sarkar, A. Langella (Eds.), Modif. Clay Zeolite Nanocomposite Mater. Environ. Pharm. Appl., Elsevier Inc., 2018, pp. 1–25, https://doi.org/10.1016/B978-0-12-814617-0.00001-3.

[13] S. Bahran, M. Ghaedi, R. Tariq, Z. Zalipour, F. Sadeghfar, Fundamental developments in the zeolite process, in: M. Ghaedi (Ed.), Photocatal. Fundam. Process. Appl., Elsevier, 2021, pp. 499–556.

[14] X. Fan, Y. Jiao, Porous materials for catalysis: toward sustainable synthesis and applications of zeolites, in: G. Szekely, A. Livingston (Eds.), Sustain. Nanoscale Eng. From Mater. Des. to Chem. Process., Elsevier Inc., 2019, pp. 115–137, https://doi.org/10.1016/B978-0-12-814681-1.00005-9.

[15] S. Belkhiri, M. Guerza, S. Chouikh, Y. Boucheffa, Z. Mekhalif, J. Delhalle, C. Colella, Textural and structural effects of heat treatment and γ-irradiation on Cs-exchanged NaX zeolite, bentonite and their mixtures, Microporous Mesoporous Mater. 161 (2012) 115–122, https://doi.org/10.1016/j.micromeso.2012.05.027.

[16] G. Cruciani, Zeolites upon heating: factors governing their thermal stability and structural changes, J. Phys. Chem. Solid. 67 (2006) 1973–1994, https://doi.org/10.1016/j.jpcs.2006.05.057.

[17] M. Jiménez-Reyes, P.T. Almazán-Sánchez, M. Solache-Ríos, Radioactive waste treatments by using zeolites. A short review, J. Environ. Radioact. 233 (2021), https://doi.org/10.1016/j.jenvrad.2021.106610.

[18] S. Kwon, C. Kim, E. Han, H. Lee, H.S. Cho, M. Choi, Relationship between zeolite structure and capture capability for radioactive cesium and strontium, J. Hazard Mater. 408 (2021) 124419, https://doi.org/10.1016/j.jhazmat.2020.124419.

[19] M. Mahima Kumar, K.A. Irshad, H. Jena, Removal of Cs+ and Sr2+ ions from simulated radioactive waste solutions using Zeolite-A synthesized from kaolin and their structural stability at high pressures, Microporous Mesoporous Mater. 312 (2021) 110773, https://doi.org/10.1016/j.micromeso.2020.110773.

[20] A. Merceille, E. Weinzaepfel, Y. Barré, A. Grandjean, The sorption behaviour of synthetic sodium nonatitanate and zeolite A for removing radioactive strontium from aqueous wastes, Separ. Purif. Technol. 96 (2012) 81–88, https://doi.org/10.1016/j.seppur.2012.05.018.

[21] H.J. Hong, B.G. Kim, J. Ryu, I.S. Park, K.S. Chung, S.M. Lee, J.B. Lee, H.S. Jeong, H. Kim, T. Ryu, Preparation of highly stable zeolite-alginate foam composite for strontium(90Sr) removal from seawater and evaluation of Sr adsorption performance, J. Environ. Manag. 205 (2018) 192–200, https://doi.org/10.1016/j.jenvman.2017.09.072.

[22] A. Kitamura, A. Kirishima, Recent activities in the field of nuclear waste management, J. Nucl. Sci. Technol. 52 (2015) 448–450, https://doi.org/10.1080/00223131.2014.952700.

[23] I. Yamagishi, R. Nagaishi, C. Kato, K. Morita, A. Terada, Y. Kamiji, R. Hino, H. Sato, K. Nishihara, Y. Tsubata, S. Tashiro, R. Saito, T. Satoh, J. Nakano, W. Ji, H. Fukushima, S. Sato, M. Denton, Characterization and storage of radioactive zeolite waste, J. Nucl. Sci. Technol. 51 (2014) 1044–1053, https://doi.org/10.1080/00223131.2014.924446.

[24] E.K. Papynov, Spark plasma sintering of ceramic and glass-ceramic matrices for cesium radionuclides immobilization, in: K. Narang (Ed.), Glas. Prop. Appl. Technol., Nova Science Publisher, Inc, New York, 2018, pp. 107–153. https://mail.google.com/mail/u/0/?pli=1%255Cnpapers3://publication/uuid/D84FC782-E317-4880-B951-0697213436E1.

[25] O.O. Shichalin, E.K. Papynov, V.Y. Maiorov, A.A. Belov, E.B. Modin, I.Y. Buravlev, Y.A. Azarova, A.V. Golub, E.A. Gridasova, A.E. Sukhorada, I.G. Tananaev, V.A. Avramenko, Spark plasma sintering of aluminosilicate ceramic matrices for immobilization of cesium radionuclides, Radiochemistry 61 (2019) 185–191, https://doi.org/10.1134/S1066362219020097.

[26] Y. Yang, T. Wang, Z. Zhang, Z. Ke, C. Shan, X. Cao, L. Ma, S. Peng, A novel method to convert Cs-polluted soil into pollucite-base glass-ceramics for Cs immobilization, Chem. Eng. J. 385 (2020) 123844, https://doi.org/10.1016/j.cej.2019.123844.

[27] P. Cappelletti, G. Rapisardo, B. De Gennaro, A. Colella, A. Langella, S. Fabio, D. Lee, M. De Gennaro, Immobilization of Cs and Sr in aluminosilicate matrices derived from natural zeolites, J. Nucl. Mater. 414 (2011) 451–457, https://doi.org/10.1016/j.jnucmat.2011.05.032.

[28] E.K. Papynov, O.O. Shichalin, V.Y. Mayorov, E.B. Modin, A.S. Portnyagin, I.A. Tkachenko, A.A. Belov, E.A. Gridasova, I.G. Tananaev, V.A. Avramenko, Spark Plasma Sintering as a high-tech approach in a new generation of synthesis of nanostructured functional ceramics, Nanotechnologies Russ 12 (2017) 49–61, https://doi.org/10.1134/S1995078017010086.
[29] S.B. Yarusova, O.O. Shichalin, A.A. Belov, S.A. Azon, I.Y. Buravlev, A.V. Golub, V.Y. Mayorov, A.V. Gerasimenko, E.K. Papynov, A.I. Ivanets, A.A. Buravleva, E.B. Merkulov, V.A. Nepomnyushchaya, O.V. Kapustina, P.S. Gordienko, Synthesis of amorphous KAlSi3O8 for cesium radionuclide immobilization into solid matrices using spark plasma sintering technique, Ceram. Int. (2021), https://doi.org/10.1016/j.ceramint.2021.10.164.
[30] E.K. Papynov, O.O. Shichalin, V.Y. Mayorov, V.G. Kuryavyi, T.A. Kaidalova, SPS technique for ionizing radiation source fabrication based on dense cesium-containing core, J. Hazard Mater. 369 (2019) 25–30, https://doi.org/10.1016/j.jhazmat.2019.02.016.
[31] A. Palčić, V. Valtchev, Synthesis and application of (nano) zeolites, in: Ref. Modul. Chem. Mol. Sci. Chem. Eng., Elsevier, 2021, https://doi.org/10.1016/B978-0-12-823144-9.00005-4.
[32] R.D. Ambashta, M. Sillanpää, Water purification using magnetic assistance: a review, J. Hazard Mater. 180 (2010) 38–49, https://doi.org/10.1016/j.jhazmat.2010.04.105.
[33] A.B. Bourlinos, R. Zboril, D. Petridis, A simple route towards magnetically modified zeolites, Microporous Mesoporous Mater. 58 (2003) 155–162, https://doi.org/10.1016/S1387-1811(02)00613-3.
[34] L.C.A. Oliveira, D.I. Petkowicz, A. Smaniotto, S.B.C. Pergher, Magnetic zeolites: a new adsorbent for removal of metallic contaminants from water, Water Res. 38 (2004) 3699–3704, https://doi.org/10.1016/j.watres.2004.06.008.
[35] H. Faghihian, M. Moayed, A. Firooz, M. Iravani, Evaluation of a new magnetic zeolite composite for removal of Cs^+ and Sr^{2+} from aqueous solutions: kinetic, equilibrium and thermodynamic studies, Compt. Rendus Chem. 17 (2014) 108–117, https://doi.org/10.1016/j.crci.2013.02.006.
[36] O. Falyouna, O. Eljamal, I. Maamoun, A. Tahara, Y. Sugihara, Magnetic zeolite synthesis for efficient removal of cesium in a lab-scale continuous treatment system, J. Colloid Interface Sci. 571 (2020) 66–79, https://doi.org/10.1016/j.jcis.2020.03.028.
[37] O. Eljamal, T. Shubair, A. Tahara, Y. Sugihara, N. Matsunaga, Iron based nanoparticles-zeolite composites for the removal of cesium from aqueous solutions, J. Mol. Liq. 277 (2019) 613–623, https://doi.org/10.1016/j.molliq.2018.12.115.
[38] T. Shubair, O. Eljamal, A. Tahara, Y. Sugihara, N. Matsunaga, Preparation of new magnetic zeolite nanocomposites for removal of strontium from polluted waters, J. Mol. Liq. 288 (2019) 111026, https://doi.org/10.1016/j.molliq.2019.111026.
[39] M.M. Rahman, S.C. Karmaker, A. Pal, O. Eljamal, B.B. Saha, Statistical techniques for the optimization of cesium removal from aqueous solutions onto iron-based nanoparticle-zeolite composites, Environ. Sci. Pollut. Res. 28 (2021) 12918–12931, https://doi.org/10.1007/s11356-020-11258-1.
[40] H. Faghihian, M. Moayed, A. Firooz, M. Iravani, Synthesis of a novel magnetic zeolite nanocomposite for removal of Cs^+ and Sr^{2+} from aqueous solution: kinetic, equilibrium, and thermodynamic studies, J. Colloid Interface Sci. 393 (2013) 445–451, https://doi.org/10.1016/j.jcis.2012.11.010.
[41] O.A.A. Moamen, H.A. Ibrahim, N. Abdelmonem, I.M. Ismail, Thermodynamic analysis for the sorptive removal of cesium and strontium ions onto synthesized magnetic nano zeolite, Microporous Mesoporous Mater. 223 (2016) 187–195, https://doi.org/10.1016/j.micromeso.2015.11.009.
[42] N. Lihareva, O. Petrov, L. Dimowa, Y. Tzvetanova, I. Piroeva, F. Ublekov, A. Nikolov, Ion exchange of Cs^+ and Sr^{2+} by natural clinoptilolite from bicationic solutions and XRD control of their structural positioning, J. Radioanal. Nucl. Chem. 323 (2020) 1093–1102, https://doi.org/10.1007/s10967-020-07018-7.
[43] T. Kouznetsova, A. Ivanets, V. Prozorovich, A. Hosseini-Bandegharaei, H.N. Tran, V. Srivastava, M. Sillanpää, Sorption and mechanism studies of Cu^{2+}, Sr^{2+} and Pb^{2+} ions on mesoporous aluminosilicates/zeolite composite sorbents, Water Sci. Technol. 82 (2020) 984–997, https://doi.org/10.2166/wst.2020.407.
[44] J.C. Buhl, Synthesis of a sulfate enclathrated zeolite with intermediate framework structure between sodalite and cancrinite, Zeitschrift Fur Anorg. Und Allg. Chemie. 643 (2017) 1030–1036, https://doi.org/10.1002/zaac.201700101.
[45] A.N. Sapozhnikov, V.L. Tauson, S.V. Lipko, R.Y. Shendrik, V.I. Levitskii, L.F. Suvorova, N.V. Chukanov, M.F. Vigasina, On the crystal chemistry of sulfur-rich lazurite, ideally $Na_7Ca(Al_6Si_6O_{24})(SO_4)(S_3)^{-}\cdot nH_2O$, Am. Mineral. 106 (2021) 226–234, https://doi.org/10.2138/am-2020-7317.
[46] N.V. Chukanov, A.N. Sapozhnikov, R.Y. Shendrik, M.F. Vigasina, R. Steudel, Spectroscopic and crystal-chemical features of sodalite-group minerals from gem lazurite deposits, Minerals 10 (2020) 1–23, https://doi.org/10.3390/min10111042.
[47] S.R. Kankrej, M.S. Kulkarni, A.V. Borhade, Adsorption isotherms, thermodynamics, kinetics and mechanism for the removal of Ca^{2+}, Mg^{2+} and Cu^{2+} ions onto Nosean prepared by using Coal Fly Ash, J. Environ. Chem. Eng. 6 (2018) 2369–2381, https://doi.org/10.1016/j.jece.2017.12.048.
[48] S.R. Kankrej, M.S. Kulkarni, R.P. Patil, A.V. Borhade, Kinetic and thermodynamic studies on adsorption behaviour of rhodamine B dye on nosean synthesised from coal, J. Emerg. Technol. Innov. Res. 5 (2018) 367–379.
[49] X. Ren, R. Qu, S. Liu, H. Zhao, W. Wu, H. Song, C. Zheng, X. Wu, X. Gao, Synthesis of zeolites from coal fly ash for the removal of harmful gaseous pollutants: a review, Aerosol Air Qual. Res. 20 (2020) 1127–1144, https://doi.org/10.4209/aaqr.2019.12.0651.
[50] S. Behrens, Preparation of functional magnetic nanocomposites and hybrid materials: recent progress and future directions, Nanoscale 3 (2011) 877–892, https://doi.org/10.1039/c0nr00634c.
[51] T.M. Gesing, J.-C. Buhl, Crystal structure of a carbonate-nosean Nas $[AlSiO_4]_6CO_3$, Eur. J. Mineral 10 (1998) 71–78, https://doi.org/10.1127/ejm/10/1/0071.
[52] C.H. Giles, T.H. MacEwan, S.N. Nakhwa, D. Smith, Studies in adsorption. Part XI. A system of Classi$cation of solution adsorption isotherms, and its use in diagnosis of adsorption mechanisms and in measurement of specific surface areas of solids, J. Chem. Soc. (1960) 3973–3993.
[53] J.S. Lee, J.M. Cha, H.Y. Yoon, J.K. Lee, Y.K. Kim, Magnetic multi-granule nanoclusters: a model system that exhibits universal size effect of magnetic coercivity, Sci. Rep. 5 (2015) 1–7, https://doi.org/10.1038/srep12135.
[54] B.D. Cullity, C.D. Graham, Introduction to Magnetic Materials, second ed., John Wiley & Sons, Inc., Hoboken, NJ, USA, 2008 https://doi.org/10.1002/9780470386323.